

## Retrieval of Elastic Green's Tensor near a Cylindrical Inhomogeneity from Vector Correlations

Juan A. Pérez-Ruiz<sup>1,\*</sup>, Francisco Luzón<sup>1</sup> and  
Francisco J. Sánchez-Sesma<sup>2</sup>

<sup>1</sup> *Grupo de Geofísica Aplicada, Departamento de Física Aplicada, Universidad de Almería, Cañada de San Urbano s/n, 04120-Almería, Spain.*

<sup>2</sup> *Departamento de Sismología, Instituto de Ingeniería, Universidad Nacional Autónoma de México, Cd. Universitaria, Circuito Escolar s/n, Coyoacán 04510, México D. F., Mexico.*

Received 30 January 2007; Accepted (in revised version) 6 June 2007

Available online 14 September 2007

---

**Abstract.** Multiple scattering of elastic waves in realistic media makes that average field intensities or energy densities follow diffusive processes. In such regime the successive  $P$  to  $S$  energy conversions by distributed random inhomogeneities give rise to equipartition which means that in the phase space the available elastic energy is distributed in average with equal amounts among the possible states of  $P$  and  $S$  waves. In such diffusive regime the  $P$  to  $S$  energy ratio equilibrates in an universal way independent of the particular details of the scattering. It has been demonstrated that averaging the cross correlations at any two points of an elastic medium subjected to diffuse elastic wavefields leads to the emergence of the Green function, which is the wave field that would be observed at one position if an impulsive load is applied at the other. In this work we study the problem of the retrieval of the 2D tensor elastodynamic Green function in an infinite elastic space containing a circular cylinder inclusion. We illuminate isotropically the elastic space with plane waves. We assume the spectra for both  $P$  and  $S$  waves uniform but such that the energy ratio  $E_S/E_P = (\alpha/\beta)^2$ , which is the one predicted by equipartition theory in two-dimensions. We then show that the Fourier transform of azimuthal average of the cross-correlation of motion between two points within an elastic medium is proportional to the imaginary part of the exact Green tensor function between these points. The numerical results presented here point out the possibility of detection and imaging of diffractors and resonant diffractors by cross correlation even in presence of attenuation exists.

**AMS subject classifications:** 86A15, 74J20, 74B05

**Key words:** Multiple scattering, elastic waves, elastic Green's tensor.

---

\*Corresponding author. *Email addresses:* japerez@ual.es (J. A. Pérez-Ruiz), fluzon@ual.es (F. Luzón), sesma@servidor.unam.mx (F. J. Sánchez-Sesma)

## 1 Introduction

The use of correlations of seismic noise and coda waves is becoming a subject of interest as it is now becoming clear that there is valuable information in these waves. We may track various previous developments that lead to the concept of diffuse wave fields. However, the pioneering approach of Aki (1957) is without any doubt crucial to understand the roles of seismic noise and coda. Aki studied descriptions that ranged from single and multiple scattering to radiative transfer ideas that he explored in order to explain coda envelopes (see Sato and Fehler, 1998).

The elastodynamic Green function has been recovered from the averaging of cross correlation of the isotropic elastic wavefield generated by either multiple scattering or by a large number of sources (such as microseisms) or microtemor as well (see Campillo and Paul, 2003; Shapiro and Campillo, 2004, Sabra et al., 2005; Shapiro et al., 2005, Chávez-García and Luzón, 2005). These experimental results have demonstrated the role of long range correlation. The Green function between two points is the wave field that would be observed at one position if an impulsive load is applied at the other. The accuracy of the reconstructed Green function depends critically on the duration of the signals processed. Theoretically the cross-correlations should be applied to equipartitioned fields (that are in a diffusive regime in which the net energy flux is null). This takes place after sufficiently long time to allow multiple scattering (and thus diffusion) of the wave field. Equipartition means that in the phase space the available energy is equally distributed, with fixed average amounts, among all the possible states. Extending these ideas of thermodynamics, equipartition has been introduced in acoustics and elastic wave propagation. When multiple scattering take place the energy ratios of the various modes tends to stabilize to a constant value, independent of the details of the scattering (see Ryzhik et al., 1996). The ratio of  $S$  and  $P$  energies in the equipartition regime ratio for the full elastic space in 2D and 3D has been obtained by Weaver (1982). It can be obtained using different arguments (see the Appendix in Sánchez-Sesma and Campillo, 2006).

In a recent work (Sánchez-Sesma and Campillo, 2006) the case of the full homogeneous elastic medium was studied both in 2D and 3D. In such study isotropic illumination and equipartition was assumed and it was demonstrated that the Fourier transform of the azimuthal average of the cross-correlation between the vector motions at two points within an infinite elastic space is proportional to the imaginary part of the exact Green tensor function between these points. This elastic case shows that both equipartition and isotropy of the field are necessary conditions to retrieve the exact Green function from correlations of the elastic field.

For horizontally layered medium Claerbout (1968) showed that the autocorrelation of the transmission response leads to reflection seismograms together with their time-reversed part. The source in the underground may be transient or noisy. In any case, the source signature in the reconstructed surface response is related to the autocorrelation of the source signal. Claerbout derivation was one dimensional but the idea has been applied to micro earthquake data (Daneshvar et al., 1995).

Sánchez-Sesma et al., (2007) used a representation theorem to retrieve the Green function of inhomogeneous, anisotropic elastic medium by averaging correlations of motions from diffuse, equipartitioned fields. These authors observed that the boundary of a 2D half-space produces in its interior fluctuations of energy densities that are considered as local effects of the diffuse field. Before Rickett and Claerbout (1999) conjectured for the 3D situation that "by cross-correlating noise traces recorded at two locations on the surface, we can construct the wave field that would be recorded at one of the locations if there was a source at the other". A numerical approach was followed to confirm this (Rickett and Claerbout, 1996). It was proven by Wapenaar (2003) explaining the empirical observations of the numerical modeling studies.

With the aim of studying a heterogeneous medium Wapenaar (2004) developed a relationship between the elastodynamic Green function and the cross correlation of observed wave fields that holds at the free surface of heterogeneous medium. The basis for that derivation was a reciprocity theorem of the correlation type, which relates two independent elastodynamic states (wave fields and sources) in the studied medium. Wapenaar (2004) expressions show that uncorrelated point sources at the boundary of the considered heterogeneous region may suffice to retrieve the Green function. The finite differences approach of Van Manem and Robertsson (2005) exploits this result for a 2D scalar medium.

On the other hand, Wapenaar et al., (2005) showed that in the recovering of the Green function problem, the time-reversal approach can be obtained as an approximation of the result of the reciprocity approach using a single point diffractor in a full space and acoustic scalar waves. Recently, Sánchez-Sesma et al., (2006) retrieved analytically by cross-correlation the imaginary part of the exact 2D Green function of a cylindrical inclusion for scalar *SH* waves. In order to compute the time response in this type of resonant diffractors, Sánchez-Sesma et al., (2006) used the Hilbert transform to generate the real part of this Green function. At the same time the experiments of Larose et al., (2006) in a medium with a cylindrical hole showed the feasibility of imaging small details of the medium by means of a passive time-correlation technique. The detection and imaging of diffractors and resonant diffractors is of special interest for geophysicists and engineers. For example the excitation and resonance of volcanic fluids inclusions are believed to be the origin of the long-period (LP) waves observed at many stages in volcanic activity (Fujita and Ida, 2003). The employment of the cross-correlations of seismic waves generated by long-period events for volcano monitoring is discussed by Sabra et al., (2006) who used the LP waves recorded during the Mount St. Helens 2004 eruption. Brenguier et al., (2007) using seismic noise correlations found a high velocity body following a preferential direction when constructing the 3D tomography of the Piton de la Fournaise volcano. They interpreted this observed orientation as an evidence of the preferential paths of magma injections. As resonators, volcanic magma inclusions may take various forms that can be simplified to simple geometrical inclusions as a plane, cylinder or a sphere (Hurst, 1992; Fujita and Ida, 2003).

In the present communication we deal with the problem of an inhomogeneous elastic

medium with a 2D circular cylindrical elastic inclusion subjected to a uniform random distribution of plane waves. The cross-correlation of the fields produced at two points by generic plane waves is computed, and then azimuthally averaged. We show that the average of the cross-correlation of the vector motion between two points is proportional to the imaginary part of the Green tensor between these points. Moreover, in the *P-SV* case the energy densities for *S* and *P* waves ( $E_S$ ,  $E_P$ , respectively) must satisfy the relationship  $E_S/E_P = (\alpha/\beta)^2$ , where  $\alpha, \beta$ =wave propagation velocities. This ratio, evaluated for the diffraction problem shown here, is the one predicted by equipartition in the full space too. At last, although our analytical solutions are obtained considering isotropy and equipartition of the background field, a recent work by Wapenaar (2006) shows that under very specific conditions the full Green function can be retrieved even when the illumination is one-sided.

## 2 The Green function for 2D *P-SV* case with a cylindrical inclusion

Let's start this case dealing with *P* and *SV* waves in a homogeneous, isotropic, elastic medium (see e.g. Aki and Richards, 1980). Propagation takes place in the  $x_1$ - $x_3$  (or  $x$ - $z$ ) plane. Therefore, the in-plane displacements  $u_i(x_1, x_3, t)$ , where  $i = 1, 3$ , fulfils Navier equation

$$\beta^2 \frac{\partial^2 u_i}{\partial x_j \partial x_j} + (\alpha^2 - \beta^2) \frac{\partial^2 u_j}{\partial x_i \partial x_j} = \frac{\partial^2 u_i}{\partial t^2}, \tag{2.1}$$

where  $\alpha$ =compressional wave velocity,  $\beta$ =shear wave velocity and  $t$ =time. In Eq. (2.1) the Einstein summation convention is used.

Assume now the presence of a cylindrical inclusion of radius  $a$  centered at the origin as show Fig. 1. In what follows the Green function for the in-plane or *P-SV* case is obtained. Let us remember the form of the Green's function in a homogeneous unbounded medium (e.g. Sánchez-Sesma and Campillo, 1991):

$$G_{ij}(x, y) = \frac{1}{i8\rho} \{ A\delta_{ij} - B(2\gamma_i\gamma_j - \delta_{ij}) \} \quad i, j = 1, 3, \tag{2.2}$$

where  $\rho$ =mass density,

$$A = \frac{H_0^{(2)}(qr)}{\alpha^2} + \frac{H_0^{(2)}(kr)}{\beta^2} \text{ and } B = \frac{H_2^{(2)}(qr)}{\alpha^2} - \frac{H_2^{(2)}(kr)}{\beta^2}, \tag{2.3}$$

with  $H_m^{(2)}(\bullet) = J_m(\bullet) - iY_m(\bullet)$ =Hankel function of the second kind and order  $m$  expressed in terms of the Bessel functions of the first and second kind. The *S* and *P* wavenumbers are given by  $k = \omega/\beta$  and  $q = \omega/\alpha$ , respectively.

Eq. (2.2) will be specialized to be the displacement field produced by a vertical or horizontal unit harmonic line load at  $y_1 = d$ ,  $y_3 = 0$ . Let's call  $\mathbf{y}$  the source location point.

In order to solve the problem for a cylindrical inclusion it is necessary to obtain the tensor Green function in polar coordinates using Graf's addition theorem to obtain the incident waves from a line force away from the origin in the reference system of the inclusion, as well as the waves scattered away by the inclusion and trapped inside it, if any (see Fig. 1).

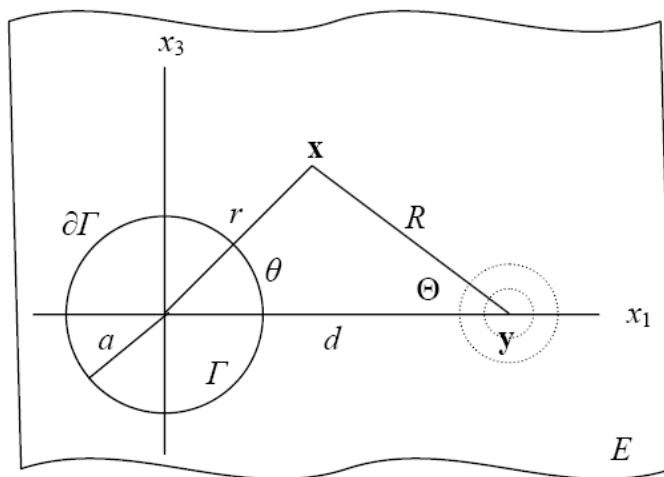


Figure 1: Configuration for the elastic circular cylinder within an infinite space. The source and receiver are located at  $y$  and  $x$ , respectively.

In order to consider the waves scattered out and refracted within the cylinder, it is possible to use the potentials  $\Phi$  and  $\Psi$  for both cases: the potentials for a horizontal force and in the case of a vertical force. Several authors have studied this problem in this sense, doing interesting contributions. Following to Pao and Mow (1973) or more recently to Mercerat et al., (2006), the displacement at point  $x$  produced by source at  $y$  is calculated, via use the Graf's addition theorem (see Abramowitz and Stegun, 1972) to modify the Hankel functions presented in potentials.

These expansion let us expressed the previous potentials for a horizontal and vertical force dependent on the coefficient  $B_m^{(x_1)(0)}$ ,  $C_m^{(x_1)(0)}$  and  $B_m^{(x_3)(0)}$ ,  $C_m^{(x_3)(0)}$  respectively. Then the potential can be used to calculate the displacements  $u$  and stresses  $\sigma$  in polar coordinates.

To obtain the Green functions when the cylindrical inclusion  $\Gamma$  is filled with an elastic material is necessary applying the continuity conditions to displacements and tractions at the boundary  $\partial\Gamma$  of the inclusion  $r = a$ . Then the scattered and refracted elastic waves are computed using the classical coefficients by Pao and Mow (1973). The needed coefficients  $B_n^{(x_j)}$ ,  $C_n^{(x_j)}$ ,  $D_n^{(x_j)}$ ,  $E_n^{(x_j)}$  for both expansions are obtained from fulfillment of boundary conditions of continuity of displacements and tractions at the interface. For a recent revision and validation see (Mercerat et al., 2006). The resolution of the generated equations' systems supplies the needed coefficients to obtain the displacements in polar coordinates.

For a horizontal point force at the region  $E$ , it is possible obtained

$$u_{r_E}^{(x_1)} = u_r^{(x_1)(0)} + u_r^{(x_1)(d)} = \sum_{n=0}^{\infty} \left[ \left( B_n^{(x_1)(0)} F_1^{J,E} + C_n^{(x_1)(0)} F_{10}^{J,E} \right) + \left( B_n^{(x_1)} F_1^{H,E} + C_n^{(x_1)} F_{10}^{H,E} \right) \right] \cos n\theta, \quad (2.4)$$

$$u_{\theta_E}^{(x_1)} = u_{\theta}^{(x_1)(0)} + u_{\theta}^{(x_1)(d)} = \sum_{n=0}^{\infty} \left[ \left( B_n^{(x_1)(0)} F_{11}^{J,E} + C_n^{(x_1)(0)} F_2^{J,E} \right) + \left( B_n^{(x_1)} F_{11}^{H,E} + C_n^{(x_1)} F_2^{H,E} \right) \right] \sin(-n\theta), \quad (2.5)$$

and at the region  $\Gamma$ ,

$$u_{r_\Gamma}^{(x_1)} = u_r^{(x_1)(r)} = \sum_{n=0}^{\infty} \left[ \left( D_n^{(x_1)} F_1^{J,\Gamma} + E_n^{(x_1)} F_{10}^{J,\Gamma} \right) \right] \cos n\theta, \quad (2.6)$$

$$u_{\theta_\Gamma}^{(x_1)} = u_{\theta}^{(x_1)(r)} = \sum_{n=0}^{\infty} \left[ \left( D_n^{(x_1)} F_{11}^{J,\Gamma} + E_n^{(x_1)} F_2^{J,\Gamma} \right) \right] \sin(-n\theta). \quad (2.7)$$

When solve the problem for a vertical point force at the region  $E$  lead to,

$$u_{r_E}^{(x_3)} = u_r^{(x_3)(0)} + u_r^{(x_3)(d)} = \sum_{n=0}^{\infty} \left[ \left( -B_n^{(x_3)(0)} F_1^{J,E} + C_n^{(x_3)(0)} F_{10}^{J,E} \right) + \left( -B_n^{(x_3)} F_1^{H,E} + C_n^{(x_3)} F_{10}^{H,E} \right) \right] \sin(-n\theta), \quad (2.8)$$

$$u_{\theta_E}^{(x_3)} = u_{\theta}^{(x_3)(0)} + u_{\theta}^{(x_3)(d)} = \sum_{n=0}^{\infty} \left[ \left( B_n^{(x_3)(0)} F_{11}^{J,E} - C_n^{(x_3)(0)} F_2^{J,E} \right) + \left( B_n^{(x_3)} F_{11}^{H,E} - C_n^{(x_3)} F_2^{H,E} \right) \right] \cos n\theta, \quad (2.9)$$

and at the region  $\Gamma$ ,

$$u_{r_\Gamma}^{(x_3)} = u_r^{(x_3)(r)} = \sum_{n=0}^{\infty} \left[ \left( -D_n^{(x_3)} F_1^{J,\Gamma} + E_n^{(x_3)} F_{10}^{J,\Gamma} \right) \right] \sin(-n\theta), \quad (2.10)$$

$$u_{\theta_\Gamma}^{(x_3)} = u_{\theta}^{(x_3)(r)} = \sum_{n=0}^{\infty} \left[ \left( D_n^{(x_3)} F_{11}^{J,\Gamma} - E_n^{(x_3)} F_2^{J,\Gamma} \right) \right] \cos n\theta. \quad (2.11)$$

Now, a simple change of coordinates leads to the Green functions of this problem,

$$G_{11}(x,y;\omega) = u_r^{(x_1)} \cos\theta - u_{\theta}^{(x_1)} \sin\theta, \quad (2.12)$$

$$G_{31}(x,y;\omega) = u_r^{(x_1)} \sin\theta + u_{\theta}^{(x_1)} \cos\theta, \quad (2.13)$$

$$G_{13}(x,y;\omega) = u_r^{(x_3)} \cos\theta - u_{\theta}^{(x_3)} \sin\theta, \quad (2.14)$$

$$G_{33}(x,y;\omega) = u_r^{(x_3)} \sin\theta + u_{\theta}^{(x_3)} \cos\theta, \quad (2.15)$$

where the references to regions  $E$  or  $\Gamma$  are omitted as these equations are valid at both regions. Now we can introduce the previous expressions for  $u_r^{(x_1)}, u_\theta^{(x_1)}, u_r^{(x_3)}, u_\theta^{(x_3)}$  in the transformed Green functions, obtaining for the region  $E$ , for example, the next expressions

$$G_{11}(x,y;\omega) = \sum_{n=0}^{\infty} \left[ \left( B_n^{(x_1)(0)} F_1^{J,E} + B_n^{(x_1)} F_1^{H,E} \right) + \left( C_n^{(x_1)(0)} F_{10}^{J,E} + C_n^{(x_1)} F_{10}^{H,E} \right) \right] \cos\theta \cos n\theta \\ + \sum_{n=0}^{\infty} \left[ \left( B_n^{(x_1)(0)} F_{11}^{J,E} + B_n^{(x_1)} F_{11}^{H,E} \right) + \left( C_n^{(x_1)(0)} F_2^{J,E} + C_n^{(x_1)} F_2^{H,E} \right) \right] \sin\theta \sin n\theta, \quad (2.16)$$

$$G_{31}(x,y;\omega) = \sum_{n=0}^{\infty} \left[ \left( B_n^{(x_1)(0)} F_1^{J,E} + B_n^{(x_1)} F_1^{H,E} \right) + \left( C_n^{(x_1)(0)} F_{10}^{J,E} + C_n^{(x_1)} F_{10}^{H,E} \right) \right] \sin\theta \cos n\theta \\ - \sum_{n=0}^{\infty} \left[ \left( B_n^{(x_1)(0)} F_{11}^{J,E} + B_n^{(x_1)} F_{11}^{H,E} \right) + \left( C_n^{(x_1)(0)} F_2^{J,E} + C_n^{(x_1)} F_2^{H,E} \right) \right] \cos\theta \sin n\theta, \quad (2.17)$$

$$G_{13}(x,y;\omega) = \sum_{n=0}^{\infty} \left[ \left( B_n^{(x_3)(0)} F_1^{J,E} B_n^{(x_3)} F_1^{H,E} \right) - \left( C_n^{(x_3)(0)} F_{10}^{J,E} + C_n^{(x_3)} F_{10}^{H,E} \right) \right] \cos\theta \sin n\theta \\ - \sum_{n=0}^{\infty} \left[ \left( B_n^{(x_3)(0)} F_{11}^{J,E} + B_n^{(x_3)} F_{11}^{H,E} \right) - \left( C_n^{(x_3)(0)} F_2^{J,E} + C_n^{(x_3)} F_2^{H,E} \right) \right] \sin\theta \cos n\theta, \quad (2.18)$$

$$G_{13}(x,y;\omega) = \sum_{n=0}^{\infty} \left[ \left( B_n^{(x_3)(0)} F_1^{J,E} B_n^{(x_3)} F_1^{H,E} \right) - \left( C_n^{(x_3)(0)} F_{10}^{J,E} + C_n^{(x_3)} F_{10}^{H,E} \right) \right] \sin\theta \sin n\theta \\ + \sum_{n=0}^{\infty} \left[ \left( B_n^{(x_3)(0)} F_{11}^{J,E} + B_n^{(x_3)} F_{11}^{H,E} \right) + \left( C_n^{(x_3)(0)} F_2^{J,E} C_n^{(x_3)} F_2^{H,E} \right) \right] \cos\theta \cos n\theta, \quad (2.19)$$

where the coefficients  $B$  and  $C$  correspond to the contribution of  $P$  and  $S$  waves respectively.

### 3 Cross-correlation in two-dimensional vector case

We proceed further to calculate the cross-correlation of the motion recorded in both points  $\mathbf{x}$  and  $\mathbf{y}$ , due to the incidence of  $P$  and  $SV$  plane waves from all possible incidence angles. Our aim is to show we can retrieve the previously derived Green function from averaging correlations. For this purpose, now the illumination is provided by incoming plane  $P$  and  $SV$  waves which are expanded in cylindrical coordinates and the corresponding scattered and refracted fields are obtained.

With reference to Fig. 2a, e.g. for incidence of  $P$  waves consider the incoming plane wave  $u_{x_3}^{(0)} = \exp(-iqx_3) \exp(i\omega t)$ ,  $u_{x_1}^{(0)} = 0$ . It can be shown that the corresponding scalar potential is simply  $\Phi_P = \frac{i}{q} \exp(-iqx_3) \exp(i\omega t)$ , which can be expanded using a Neuman's expansion in series of Bessel functions which are series of solutions of the elastic equation. Let's then resort to the potentials for each case, in order to considerer the waves

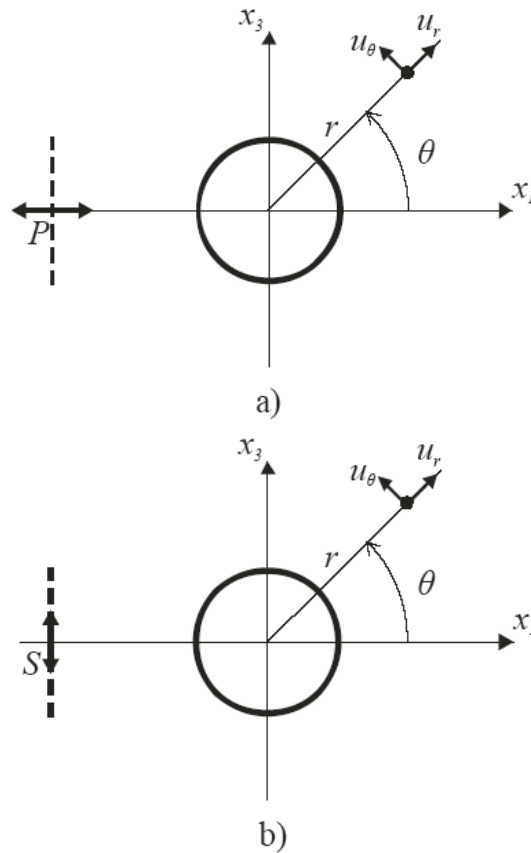


Figure 2: a) scheme of incidence of  $P$  plane wave, b) scheme of incidence of  $S$  plane wave.

scattered out and refracted within the cylinder. Now we use the potential  $\Phi$  for  $P$  waves and  $\Psi$  for  $S$  waves. In the first case the potential is

$$\Phi_P = \frac{i}{q} \sum_{n=0}^{\infty} (-i)^n \varepsilon_n J_n(qr) \cos n\theta. \quad (3.1)$$

When an  $S$  wave is propagated, the potential has the form

$$\Psi_S = \frac{-i}{k} \sum_{n=0}^{\infty} (-i)^n \varepsilon_n \frac{n}{r} J_n(kr) \sin n\theta. \quad (3.2)$$

Now it is possible to determine the displacements and stresses from these potentials. After some algebra we achieve the following expressions for the free field in the  $P$  wave case,

$$u_r^{P(0)} = \sum_{n=0}^{\infty} B_n^{P(0)} J'_n(qr) \cos n\theta, \quad (3.3)$$

$$u_\theta^{P(0)} = \sum_{n=0}^{\infty} B_n^{P(0)} \frac{n}{r} J_n(qr) \sin(-n\theta), \quad (3.4)$$

and these other expressions for the free field in the  $S$  wave case,

$$u_r^{S(0)} = \sum_{n=0}^{\infty} C_n^{S(0)} \frac{n}{r} J_n(kr) \sin(-n\theta), \quad (3.5)$$

$$u_{\theta}^{S(0)} = \sum_{n=0}^{\infty} C_n^{S(0)} J'_n(kr) \cos n\theta, \quad (3.6)$$

where the coefficients  $B_n^{P(0)}$  and  $C_n^{P(0)}$  are defined as

$$B_n^{P(0)} = \frac{i}{q} (-i)^n \varepsilon_n, \quad (3.7)$$

$$C_n^{S(0)} = \frac{-i}{k} (-i)^n \varepsilon_n. \quad (3.8)$$

Again it is necessary to apply the conditions of continuity of displacements and stresses in order to work out the value of the coefficients needed to calculate the diffracted and refracted fields. This leads to a linear system of order 4 for each  $n$  (for  $n=0$  the order is 2, which means there are only  $P$  waves for  $n=0$ ) to retrieve the expansion coefficients  $B_n^T, C_n^T, D_n^T, E_n^T$ , as in the previous punctual force section, but in this case  $T$  represent the kind of the wave  $P$  or  $S$ . When the  $P$  plane wave is treated this system let to express the complete solution for  $P$  wave at the region  $E$  as

$$u_{r_E}^P = u_r^{P(0)} + u_r^{(d)} = \sum_{n=0}^{\infty} \left[ \left( B_n^{P(0)} F_1^{J,E} \right) + \left( B_n^P F_1^{H,E} + C_n^P F_{10}^{H,E} \right) \right] \cos n\theta, \quad (3.9)$$

$$u_{\theta_E}^P = u_{\theta}^{P(0)} + u_{\theta}^{(d)} = \sum_{n=0}^{\infty} \left[ \left( B_n^{P(0)} F_{11}^{J,E} \right) + \left( B_n^P F_{11}^{H,E} + C_n^P F_2^{H,E} \right) \right] \sin(-n\theta), \quad (3.10)$$

and at the region  $\Gamma$  as

$$u_{r_{\Gamma}}^P = u_r^{(r)} = \sum_{n=0}^{\infty} \left[ \left( D_n^P F_1^{J,\Gamma} + E_n^P F_{10}^{J,\Gamma} \right) \right] \cos n\theta, \quad (3.11)$$

$$u_{\theta_{\Gamma}}^P = u_{\theta}^{(r)} = \sum_{n=0}^{\infty} \left[ \left( D_n^P F_{11}^{J,\Gamma} + E_n^P F_2^{J,\Gamma} \right) \right] \sin(-n\theta), \quad (3.12)$$

where the functions  $F$  are presented in Appendix A. On the other hand, when the  $S$  plane wave is treated the solution for  $S$  plane wave at the region  $E$  is

$$u_{r_E}^S = u_r^{S(0)} + u_r^{(d)} = \sum_{n=0}^{\infty} \left[ \left( C_n^{S(0)} F_{10}^{J,E} \right) + \left( -B_n^S F_1^{H,E} + C_n^S F_{10}^{H,E} \right) \right] \sin(-n\theta), \quad (3.13)$$

$$u_{\theta_E}^S = u_{\theta}^{S(0)} + u_{\theta}^{(d)} = \sum_{n=0}^{\infty} \left[ \left( -C_n^{S(0)} F_2^{J,E} \right) + \left( B_n^S F_{11}^{H,E} - C_n^S F_2^{H,E} \right) \right] \cos n\theta, \quad (3.14)$$

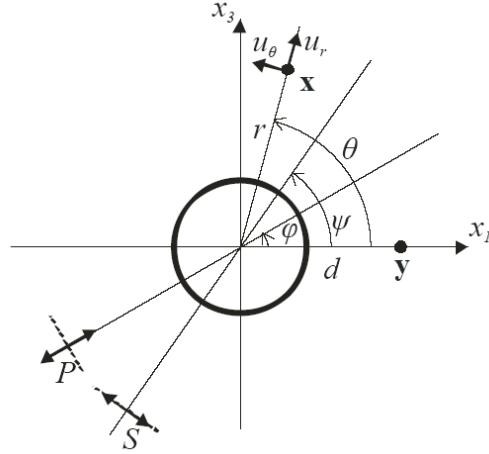


Figure 3: Detail of the illumination of the cylindrical inclusion for plane waves.

and at the region  $\Gamma$  as

$$u_{r\Gamma}^S = u_r^{(r)} = \sum_{n=0}^{\infty} \left[ \left( -D_n^S F_1^{J,\Gamma} + E_n^S F_{10}^{J,\Gamma} \right) \right] \sin(-n\theta), \tag{3.15}$$

$$u_{\theta\Gamma}^S = u_{\theta}^{(r)} = \sum_{n=0}^{\infty} \left[ \left( D_n^S F_{11}^{J,\Gamma} - E_n^S F_2^{J,\Gamma} \right) \right] \cos n\theta. \tag{3.16}$$

Let's hereafter the reference to region  $E$  or  $\Gamma$  be omitted, it is supposed to be in the interest region. In order to assure the illumination from all angles we express the displacements as (see Fig. 3)

$$u_r = P \sum_n u_r^P \cos n(\theta - \varphi) + S \sum_m u_r^S (-\sin m(\theta - \psi)), \tag{3.17}$$

$$u_{\theta} = P \sum_n u_{\theta}^P (-\sin n(\theta - \varphi)) + S \sum_m u_{\theta}^S \cos m(\theta - \psi), \tag{3.18}$$

where the contribution of  $P$  and  $S$  waves are jointly considered. Here  $P$  or  $S$  are the complex waveform  $F(\omega, \chi)$ , being  $\chi$  the incident angle  $\varphi$  or  $\psi$  depending on case. Let us assume  $F(\omega, \chi)$  independent of incoming angle to become simply  $F(\omega)$ . This choice means we assume isotropy of the background illumination.

It is convenient to change of coordinates to come back to Cartesian axis via

$$u_{x_1} = u_r \cos \theta - u_{\theta} \sin \theta, \tag{3.19}$$

$$u_{x_3} = u_r \sin \theta + u_{\theta} \cos \theta. \tag{3.20}$$

Expressions for the cross-correlations are then obtained. For this aim we need the dis-

placements at the point  $\mathbf{x}(r, \theta)$

$$u_{x_1}(r, \theta) = P \sum_n \left[ u_r^P \cos \theta \cos n(\theta - \varphi) + u_\theta^P (\sin \theta \sin n(\theta - \varphi)) \right] \\ + S \sum_m \left[ u_r^S (-\cos \theta \sin m(\theta - \psi)) + u_\theta^S (-\sin \theta \cos m(\theta - \psi)) \right], \quad (3.21)$$

$$u_{x_3}(r, \theta) = P \sum_n \left[ u_r^P \sin \theta \cos n(\theta - \varphi) + u_\theta^P (-\cos \theta \sin n(\theta - \varphi)) \right] \\ + S \sum_m \left[ u_r^S (-\sin \theta \sin m(\theta - \psi)) + u_\theta^S (\cos \theta \cos m(\theta - \psi)) \right], \quad (3.22)$$

and the complex conjugate of the displacements at the point  $\mathbf{y}(d, 0)$

$$u_{x_1}^*(d, 0) = P^* \sum_n \left[ u_r^{P*} \cos n\varphi \right] + S^* \sum_m \left[ u_r^{S*} \sin m\psi \right], \quad (3.23)$$

$$u_{x_3}^*(d, 0) = P^* \sum_n \left[ u_\theta^{P*} \sin n\varphi \right] + S^* \sum_m \left[ u_\theta^{S*} \cos m\psi \right]. \quad (3.24)$$

Now we are in conditions to do the cross-correlation of these displacements. We have assumed an isotropic field. This allows to do the azimuthal average over these angles. This average implicates several integrals which lead to

$$\int_0^{2\pi} \cos mx \cos nx dx = \left( \frac{1}{\varepsilon_n} \right) \delta_{mn}, \quad \int_0^{2\pi} \sin mx \sin nx dx = \left( \frac{\varepsilon_n - 1}{\varepsilon_n} \right) \delta_{mn}$$

(no summation), and then after some algebra, we have:

$$\langle u_{x_1}(r, \theta) \cdot u_{x_1}^*(d, 0) \rangle = \left( P^2 \sum_n u_r^P u_r^{P*} \left( \frac{1}{\varepsilon_n} \right) + S^2 \sum_n u_r^S u_r^{S*} \left( \frac{\varepsilon_n - 1}{\varepsilon_n} \right) \right) \cos \theta \cos n\theta \\ + \left( P^2 \sum_n u_\theta^P u_\theta^{P*} \left( \frac{1}{\varepsilon_n} \right) - S^2 \sum_n u_\theta^S u_\theta^{S*} \left( \frac{\varepsilon_n - 1}{\varepsilon_n} \right) \right) \sin \theta \sin n\theta, \quad (3.25)$$

$$\langle u_{x_3}(r, \theta) \cdot u_{x_1}^*(d, 0) \rangle = \left( P^2 \sum_n u_r^P u_r^{P*} \left( \frac{1}{\varepsilon_n} \right) + S^2 \sum_n u_r^S u_r^{S*} \left( \frac{\varepsilon_n - 1}{\varepsilon_n} \right) \right) \sin \theta \cos n\theta \\ - \left( P^2 \sum_n u_\theta^P u_\theta^{P*} \left( \frac{1}{\varepsilon_n} \right) - S^2 \sum_n u_\theta^S u_\theta^{S*} \left( \frac{\varepsilon_n - 1}{\varepsilon_n} \right) \right) \cos \theta \sin n\theta, \quad (3.26)$$

$$\langle u_{x_1}(r, \theta) \cdot u_{x_3}^*(d, 0) \rangle = \left( P^2 \sum_n u_r^P u_\theta^{P*} \left( \frac{\varepsilon_n - 1}{\varepsilon_n} \right) - S^2 \sum_n u_r^S u_\theta^{S*} \left( \frac{1}{\varepsilon_n} \right) \right) \cos \theta \sin n\theta \\ - \left( P^2 \sum_n u_\theta^P u_\theta^{P*} \left( \frac{\varepsilon_n - 1}{\varepsilon_n} \right) + S^2 \sum_n u_\theta^S u_\theta^{S*} \left( \frac{1}{\varepsilon_n} \right) \right) \sin \theta \cos n\theta, \quad (3.27)$$

$$\begin{aligned} \langle u_{x_3}(r,\theta) \cdot u_{x_3}^*(d,0) \rangle = & \left( P^2 \sum_n u_r^P u_\theta^{P*} \left( \frac{\varepsilon_n - 1}{\varepsilon_n} \right) - S^2 \sum_n u_r^S u_\theta^{S*} \left( \frac{1}{\varepsilon_n} \right) \right) \sin\theta \sin n\theta \\ & + \left( P^2 \sum_n u_\theta^P u_\theta^{P*} \left( \frac{\varepsilon_n - 1}{\varepsilon_n} \right) + S^2 \sum_n u_\theta^S u_\theta^{S*} \left( \frac{1}{\varepsilon_n} \right) \right) \cos\theta \cos n\theta. \end{aligned} \quad (3.28)$$

We found that the integrals involving the products of the factors  $P$  by  $S$  are null. Remember the previous expressions (2.16) to (2.19) for Green functions; it is possible to observe the similitude among these expressions and cross-correlation (3.25) to (3.28). Developing the expressions (3.25) to (3.28), for region  $E$  or  $\Gamma$ , the real character of the cross-correlation is easy to find. Then, computing both tensor quantities, the Green function and the cross-correlation of the displacements register at the two chosen points, we find a relation among imaginary part of Green functions and the cross-correlation. This allows checking the relation developed by Sánchez-Sesma et al. (2006). In this work the ratio between the Green function and cross-correlation is presented as

$$\langle u_i(\mathbf{y},\omega) u_j^*(\mathbf{x},\omega) \rangle = -8E_S k^{-2} \text{Im} [G_{ij}(\mathbf{x},\mathbf{y},\omega)], \quad (3.29)$$

where the equipartition theory is assumed, that is assuming the spectra for both  $P$  and  $S$  uniform and such that the energy ratio is  $E_S/E_P = \alpha^2/\beta^2$ . Here  $E_S = \rho\omega^2 S^2/2$  and  $E_P = \rho\omega^2 P^2/2$ . The result is the extension of the scalar  $SH$  case Sánchez-Sesma et al. (2006) and is also identical to the result reported by Sánchez-Sesma and Campillo (2006) for the 2D vector case in the full homogeneous space for  $P$  and  $S$  waves.

In order to illustrate this identity, we consider with various examples and retrieve the Green functions by means of the methodology presented herein.

## 4 Computational procedure

By means of the methodology here presented, in next epigraph we deal with various examples testing the relation (3.29). The suitable implementation of the theory presented in previous section is necessary. In this way, the needed computational time to compute the cross-correlation is comparable to necessary time to calculate the analytical solution. In order to achieve this aim, the Fortran language is used. Next, the algorithm employed to compute the cross-correlation of the planar wave contribution is presented.

With Algorithm 4.1, only a few terms of the series are needed to achieve a reliable result. When the velocity contrast between the inclusion and the surrounding medium is high, approximately  $\sim 60$  series terms are needed. Nevertheless, when a homogeneous medium is computed only  $\sim 25$  series terms are necessary. The cross-correlation procedure is a low cost subroutine, and it is much faster than other numerical algorithms as finite differences method or finite element method.

Algorithm 4.1: *xcorr*

---

**C COMPUTING THE PLANE WAVE CONTRIBUTION**

```

Define  $q_e, k_e, q_r, k_r$ 
for series expansion from 1 to end series limit
  call functions  $F_e$ 
  call functions  $F_r$ 
  prepare the equation system to P-waves
  call solve the system
  prepare the equation system to S-waves
  call solve the system
end

```

**C COMPUTING THE RESPONSE IN RECEIVERS 1 AND 2**

```

for receivers from 1 to 2
  define  $r$ 
  if  $r > ra$ 
    P-wave field = P-free field + diffracted field
  else if  $r < ra$ 
    P-wave field = refracted field
  if  $r > ra$ 
    S-wave field = S-free field + diffracted field
  else if  $r < ra$ 
    S-wave field = refracted field
  total contribution = P-wave field + S-wave field
end

```

**C COMPUTING THE CROSS-CORRELATION BETWEEN  $\mathbf{x}$  AND  $\mathbf{y}$** 

```

initialize data
for series expansion from 1 to series limit
  Compute  $xcorr_{11}$  Eq. (3.25)
  Compute  $xcorr_{31}$  Eq. (3.26)
  Compute  $xcorr_{13}$  Eq. (3.27)
  Compute  $xcorr_{33}$  Eq. (3.28)
end

```

**C WRITING THE RESULTS**

---

This process allows deal with real data easily. Recent works, as Brenguier et al. (2007), show the use of this technique in order to make velocity maps by tomography with real data. Other interesting application of this procedure is the volcano monitoring, as it is shown in the work of Sabra et al. (2006).

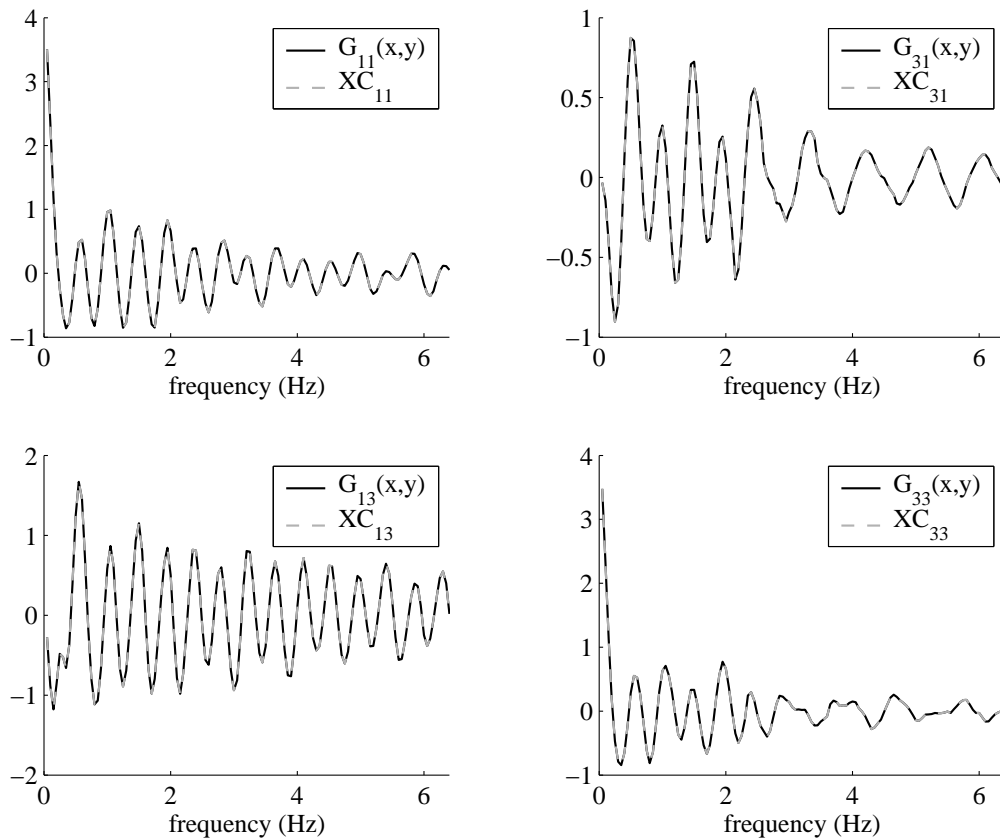


Figure 4: Solid black lines depict the imaginary parts of the tensor Green function ( $G_{ij}$ ). The dashed gray lines are the average cross-correlations ( $XC_{ij}$ ) between the displacements recorded at points  $x$  and  $y$ . For numerical reasons both quantities are represented divided by the square of the wave velocity.

## 5 Numerical examples

In the previous sections the analytical solution for the Green function retrieval from correlations was made explicit for a classical problem of dynamic elasticity in 2D. Now, we want to show the relationship between the tensor Green function in frequency domain and the Fourier transform of the azimuthal average of the tensor cross-correlation of the motion at two points in an inhomogeneous medium. This domain is formed by a cylindrical inclusion embedded in an infinite elastic space. The motion is consequence of uniform illumination of plane waves.

Consider the in-plane  $P$ - $SV$  case and refer to Fig. 1, with a stiffer inclusion at the medium. We assumed the exterior  $E$  with  $S$ -wave velocity  $\beta_E = 0.4 \text{ km/s}$ ,  $P$ -wave velocity  $\alpha_E = 0.8 \text{ km/s}$  and mass density  $\rho_E = 2.1 \text{ g/cm}^3$ , while the cylindrical inclusion  $\Gamma$  has a radius  $a = 0.5 \text{ km}$  and  $S$ -wave velocity  $\beta_\Gamma = 0.7 \text{ km/s}$ ,  $P$ -wave velocity  $\alpha_\Gamma = 1.2 \text{ km/s}$  and mass density  $\rho_\Gamma = 2.4 \text{ g/cm}^3$ . Two receivers are placed in this model at the points  $x$  and

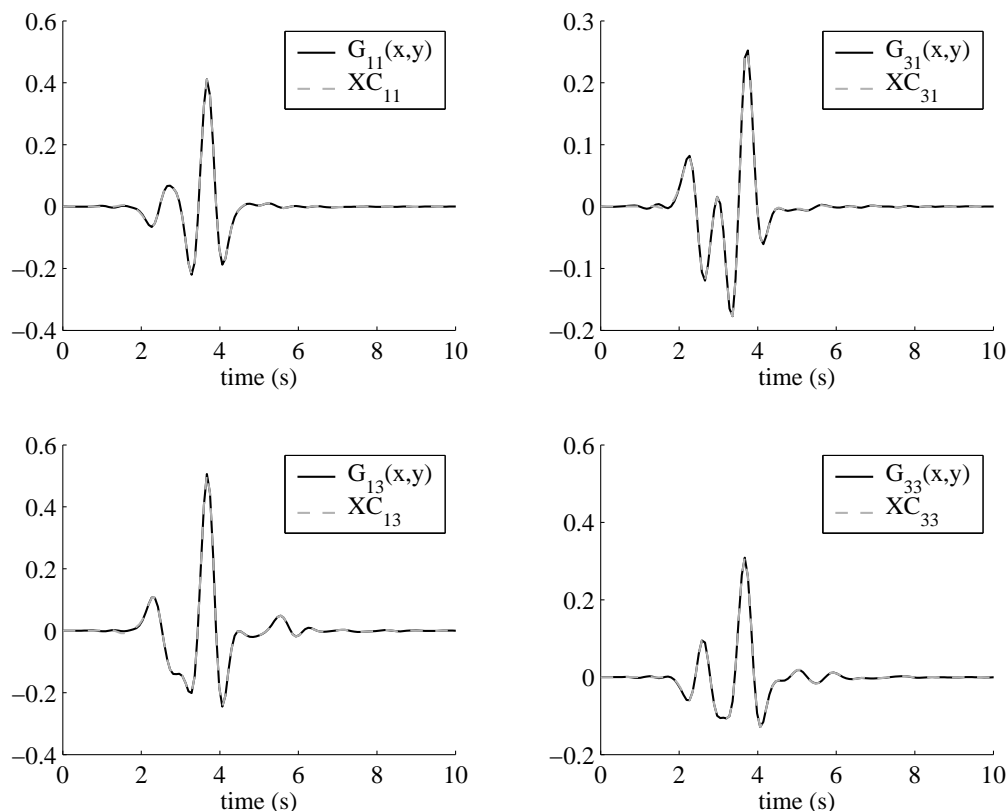


Figure 5: The solid traces are the synthetic seismograms from the analytical Green function while dashed gray lines depict the synthetic seismogram from cross-correlations and their Hilbert transforms.

$y$ . The point  $y$  is separated a distance  $d = 1.0\text{km}$  from the origin with zero azimuth. The point  $x$  is placed at  $r = 0.75\text{km}$  and  $\theta = 60$  degrees. In Fig. 4 both members of Eq. (3.29) divided by the square of wave velocity are depicted. The black solid line represents the right member, and the dashed gray line depicts the left member of the equation. Calculations were done for 128 frequencies up to 6.4 Hz and the number of terms in the wave functions expansions varies linearly with frequency from 15 to 55 terms. It is possible to observe an excellent agreement. The effects of heterogeneity are clearly visible in the faint oscillations of  $\text{Im}[G_{ij}]$ , which reveals the resonances of the energy trapped within the inclusion.

Fig. 5 displays synthetic seismograms. They are computed from convolving a Ricker wavelet (with characteristic period  $t_p = 1.0\text{s}$ ) with the analytic Green tensor and the cross-correlations, respectively. The traces are superimposed and we can observe a very good agreement between both sets of synthetics. We have used the Hilbert transform to generate the real parts of the tensor Green function which comes from the average of cross-correlations.

Now the same geometry with a softer inclusion is considered. In this model the ex-

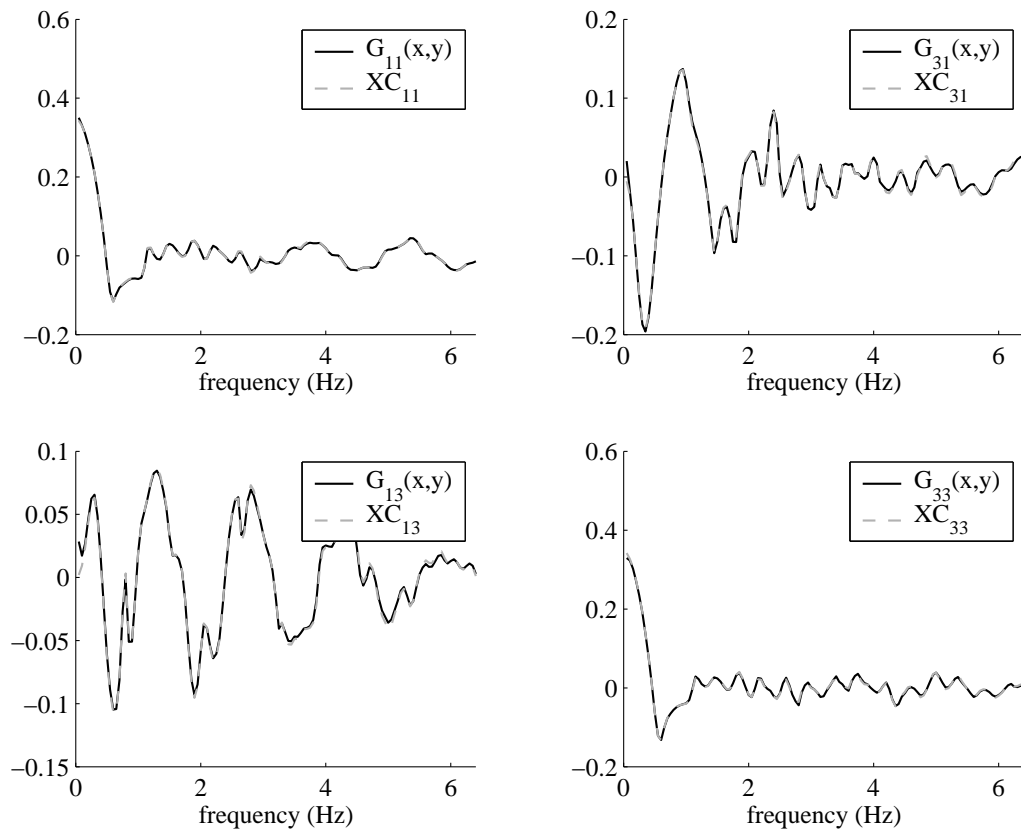


Figure 6: Solid black lines depict the imaginary parts of the tensor Green function ( $G_{ij}$ ). The dashed gray lines are the average cross-correlations ( $XC_{ij}$ ) between the displacements recorded at points  $x$  and  $y$ . For numerical reasons both quantities are represented divided by the square of the wave velocity.

terior region  $E$  has a  $S$ -wave velocity  $\beta_E = 1.5 \text{ km/s}$ ,  $P$ -wave velocity  $\alpha_E = 2.0 \text{ km/s}$  and mass density  $\rho_E = 2.3 \text{ g/cm}^3$ , whereas the cylindrical inclusion  $\Gamma$  has a radius  $a = 0.5 \text{ km}$  and  $S$ -wave velocity  $\beta_\Gamma = 0.7 \text{ km/s}$ ,  $P$ -wave velocity  $\alpha_\Gamma = 1.0 \text{ km/s}$  and mass density  $\rho_\Gamma = 2.1 \text{ g/cm}^3$ . In this case the point  $x$  is placed at  $r = 0.75 \text{ km}$  and  $\theta = 90$  degrees while the point  $y$  is separated a distance  $d = 1.0 \text{ km}$  from the origin with zero azimuth. In order to analyze the effects of the attenuation, in this example the region  $E$  has a quality factor  $Q_P = 200$  and  $Q_S = 150$ , whereas the region  $\Gamma$  has a quality factor  $Q_P = 100$  and  $Q_S = 80$ . In Fig. 6 the imaginary part of the four components of the tensor Green function are presented together with the real part of the average cross-correlation of the displacements recorded at both receivers. In this case, some differences appear in the results. The averaging cross-correlation does not retrieve exactly the tensor Green function, nevertheless the level of misfits is very low. This is in agreement with the recent results by Snieder et al. (2007) that the Green function can be retrieved from the response to random forcing for a variety of conditions, including the extreme case of the diffusion equation.

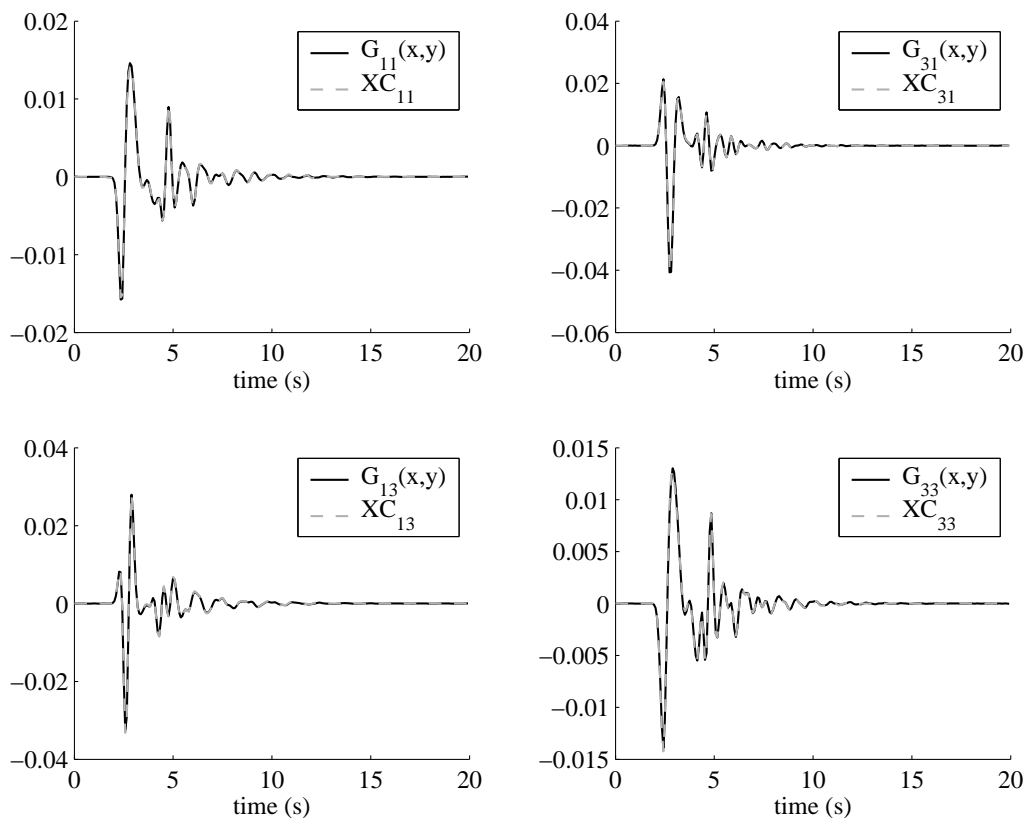


Figure 7: The solid traces are the synthetic seismograms from the analytical Green function while dashed gray lines depict the synthetic seismogram from cross-correlations and their Hilbert transforms.

Fig. 7 show synthetic seismograms generated from convolution of a Ricker wavelet (with characteristic period  $t_p = 0.75s$ ) with the analytic Green tensor and the cross-correlations, respectively. As in the model within a stiffer inclusion, although in this case, the attenuation is taken into account, it is possible observe a good agreement between the traces generated by Green functions and those computed by real part of cross-correlations and its Hilbert transform.

It is interesting to test the misfit between both traces in a quantitative way. For this aim the formulation of Kristekova et al. (2006) is employed. This formulation presents the envelope and phase misfit separately. Using these magnitudes to evaluate the misfits, we find the misfits presented in Table 1.

These results for the Green tensor show the generality of our result. Inclusive when the attenuation is taken into account the cross-correlation retrieves the Green function with an agreement larger than 96-97 %. It is a very important result, since the real media present attenuation, and this procedure is suitable to retrieval approximately the components of the Green tensor in this kind of the media. For an unbounded elastic space

Table 1: Envelope and phase misfits corresponding to Green tensor components and the cross-correlations for the stiffer inclusion problem.

	Envelope Misfit (%)	Phase Misfit (%)
$G_{11}$	2.98	0.83
$G_{31}$	2.75	1.02
$G_{13}$	2.26	0.59
$G_{33}$	3.42	1.37

it is well-known that the Green function  $G_{ij}(\mathbf{x}, \mathbf{y})$  is a symmetric tensor. However, the elastodynamic Green tensor for a heterogeneous medium or for a homogeneous body with boundaries is no longer symmetric. In fact, for our heterogeneous problem we have verified that  $G_{ij}(\mathbf{x}, \mathbf{y}, \omega) \neq G_{ji}(\mathbf{x}, \mathbf{y}, \omega)$  and, as a consequence of reciprocity, the identity  $G_{ij}(\mathbf{x}, \mathbf{y}, \omega) \equiv G_{ji}(\mathbf{y}, \mathbf{x}, \omega)$ ,  $i \neq j$ , is fulfilled as well.

## 6 Conclusion

The retrieval of 2D heterogeneous Green function of an elastic cylindrical inclusion embedded in an infinite homogeneous, elastic medium which is illuminated by isotropic random wavefield that satisfies the equipartition ratio (in the  $P$ - $SV$  case) has been obtained. The equipartition of the energy carried by diffuse elastic waves in 2D is given by the relationship  $E_S = (\alpha/\beta)^2 E_P$ , where  $E_S$  and  $E_P$  are the  $S$  and  $P$  spatial energy densities, and  $\alpha$  and  $\beta$  are the  $P$  and  $S$  wave speeds, respectively.

In order to thoroughly validate this important finding for the  $P$ - $SV$  inplane problem the computations are done numerically over the analytical expressions. We used the Graf's addition theorem to translate the line forces' potentials (given by expressions of the form  $H_1^{(2)}(kR)\cos\Theta$  and  $H_1^{(2)}(kR)\sin\Theta$  at the point of load application) into expansions at the cylinder origin. The Pao and Mow (1973) coefficients for all the displacements and stresses in cylindrical coordinates have to be used and the fields numerically computed. In developing the codes sometimes certain calculations were done numerically for verification purposes. With this procedure, for this composite medium we retrieve, from the correlations of the field produced by the isotropic and equipartitioned elastic background, the exact Green function. The results presented in the present communication for a cylindrical inclusion verify and extend the validity of our previous results for the homogeneous, unbounded elastic space.

The usefulness of correlations is not confined to the retrieval of the Green function. Indeed, correlations do provide significant, useful information even in cases where the diffuse nature of the fields is not at all obvious. An implication of the present findings is that being the cylindrical inclusion embedded in a full space the equipartitioned, isotropic illumination (a background radiation) is independent of the scatter but the local equipartitioned regime already includes its effects. The numerical results presented here point

out also the possibility of detection and imaging of diffractors and resonant diffractors by cross correlation of real records even if attenuation exists.

## Acknowledgments

Partial supports from project CGL2005-05500-C02-02/BTE from CICYT, Spain; from the EU with FEDER; and the Research Team RNM-194 of Junta de Andalucía, Spain; from CONACYT, Mexico, under grant NC-204; from DGAPA-UNAM, Mexico, under grant IN114706, are gratefully acknowledged. The help of G. Sánchez and her USI team has been crucial to locate various references.

## Appendix A

Function's catalogue follows the expressions based on Pao and Mow (1973). In these expressions  $Z$  represents the corresponding Bessel  $J$  or Hankel  $H$  functions.  $L$  corresponds to the region ( $E$  or  $\Gamma$ ) where the displacement is calculated, and the  $S$  and  $P$  wavenumbers are given by  $k_L = \omega / \beta_L$  and  $q_L = \omega / \alpha_L$ , respectively.

$$\begin{aligned}
 F_1^{Z,L} &= \frac{n}{r} Z_n(q_L r) - q_L Z_{n+1}(q_L r), \\
 F_2^{Z,L} &= \frac{n}{r} Z_n(k_L r) - k_L Z_{n+1}(k_L r), \\
 F_3^{Z,L} &= \left( \frac{n^2 - n}{r^2} - q_L^2 \right) Z_n(q_L r) - \frac{q_L}{r} Z_{n+1}(q_L r), \\
 F_4^{Z,L} &= \left( \frac{n^2 - n}{r^2} - k_L^2 \right) Z_n(k_L r) - \frac{k_L}{r} Z_{n+1}(k_L r), \\
 F_5^{Z,L} &= -q_L^2 Z_n(q_L r), \\
 F_6^{Z,L} &= \frac{1}{r^2} \left[ \left( n^2 - n - \frac{k_L^2 r^2}{2} \right) Z_n(k_L r) - k_L r Z_{n+1}(k_L r) \right], \\
 F_7^{Z,L} &= \frac{1}{r^2} \left[ (n^2 - n) Z_n(q_L r) - n q_L r Z_{n+1}(q_L r) \right], \\
 F_8^{Z,L} &= \frac{1}{r^2} \left[ (n^2 - n) Z_n(k_L r) - n k_L r Z_{n+1}(k_L r) \right], \\
 F_9^{Z,L} &= Z_n(q_L r), \\
 F_{10}^{Z,L} &= \frac{n}{r} Z_n(k_L r), \\
 F_{11}^{Z,L} &= \frac{n}{r} Z_n(q_L r), \\
 F_{13}^{Z,L} &= \frac{1}{r^2} \left[ \left( n^2 - n - \frac{\alpha^2}{2\beta^2} q_L^2 r^2 \right) Z_n(q_L r) - q_L r Z_{n+1}(q_L r) \right].
 \end{aligned}$$

## References

- [1] M. Abramowitz and I. A. Stegun, *Handbook of Mathematical Functions*, Dover Publications Inc., New York, 1972.
- [2] K. Aki, Space and time spectra of stationary stochastic waves with special reference to microtremors, *Bull. Earthq. Res. Inst.*, 35 (1957), 415-456.
- [3] K. Aki and P. G. Richards, *Quantitative Seismology*, W. H. Freeman and Co., San Francisco, 1980.
- [4] F. Brenguier, N. M. Shapiro, M. Campillo, A. Nercessian and V. Ferrazzini, 3-D wave tomography of the Piton de la Fournaise volcano using seismic noise correlations, *Geophys. Res. Lett.*, 34 (2007), L02305.
- [5] M. Campillo and A. Paul, Long range correlations in the seismic coda, *Science*, 299 (2003), 547-549.
- [6] F. Chávez-García and F. Luzón, On the correlation of seismic microtremors, *J. Geophys. Res.*, 110 (2005), doi:10.1029/2005JB003671.
- [7] J. F. Claerbout, Synthesis of a layered medium from its acoustic transmission response, *Geophysics*, 33 (1968), 264-269.
- [8] M. R. Daneshvar, C. S. Clay and M. K. Savage, Passive seismic imaging using microearthquakes, *Geophysics*, 60 (1995), 1178-1186.
- [9] E. Fujita and Y. Ida, Geometrical effects and low-attenuation resonance of volcanic fluid inclusions for the source mechanism of long-period earthquakes, *J. Geophys. Res.*, 108 (2003), doi:10.1029/2002JB001806.
- [10] A. W. Hurst, Stochastic simulation of volcanic tremor from Ruapehu, *J. Volcanol. Geoth. Res.*, 51 (1992), 185-198.
- [11] M. Kristekova, J. Kristek, P. Moczo and S. M. Day, Misfit criteria for quantitative comparison of seismograms, *Bull. Seism. Soc. Am.*, 96 (2006), 1836-1850.
- [12] E. Larose, O. I. Lobkis and R. L. Weaver, Passive correlation imaging of a buried scatterer (L), *J. Acoust. Soc. Am.*, 119(6) (2006), 3549-3552.
- [13] E. D. Mercerat, J.-P. Vilotte and F. J. Sánchez-Sesma, Triangular spectral element simulation of 2D elastic wave propagation using unstructured triangular grids, *Geophys. J. Int.*, 166 (2006), 679-698.
- [14] Y.-H. Pao and C.-C. Mow, *Diffraction of Elastic Waves and Dynamics Stress Concentrations*, Crane Russak/Adam Hilger, 1973.
- [15] J. Rickett and J. Claerbout, Passive seismic imaging applied to synthetic data, *Stanford Exploration Project*, 92 (1996), 83-90.
- [16] J. Rickett and J. Claerbout, Acoustic daylight imaging via spectral factorization: Helioseismology and reservoir monitoring, *The Leading Edge*, 18 (1999), 957-960.
- [17] L. V. Ryzhik, G. C. Papanicolau and J. B. Keller, Transport equations for elastic and other waves in random media, *Wave Motion*, 24 (1996), 327-370.
- [18] K. G. Sabra, P. Gerstoft, P. Roux, W. A. Kuperman and M. C. Fehler, Extracting time-domain Green's function estimates from ambient seismic noise, *Geophys. Res. Lett.*, 32 (2005), L03310.
- [19] K. G. Sabra, P. Roux, P. Gerstoft, W. A. Kuperman and M. C. Fehler, Extracting coherent coda arrivals from cross-correlations of long period seismic waves during the Mount St. Helens 2004 eruption, *Geophys. Res. Lett.*, 33 (2006), L06313.
- [20] F. J. Sánchez-Sesma and M. Campillo, Diffraction of P, SV and Rayleigh waves by topographic features: a boundary integral formulation, *Bull. Seism. Soc. Am.*, 81 (1991), 2234-

2253.

- [21] F. J. Sánchez-Sesma and M. Campillo, Retrieval of the Green function from cross-correlation: The canonical elastic problem, *Bull. Seism. Soc. Am.*, 96 (2006), 1182-1191.
- [22] F. J. Sánchez-Sesma, J. A. Pérez-Ruiz, M. Campillo and F. Luzón, Elastodynamic 2D Green function retrieval from cross-correlation: Canonical inclusion problem, *Geophys. Res. Lett.*, 33 (2006), L13305.
- [23] F. J. Sánchez-Sesma, J. A. Pérez-Ruiz, F. Luzón, M. Campillo and A. Rodríguez-Castellanos, Diffuse fields in dynamic elasticity, *Wave Motion*, (2007), doi:10.1016/j.wavemoti.2007.07.005.
- [24] H. Sato and M. Fehler, *Wave Propagation and Scattering in the Heterogeneous Earth*, Springer-Verlag, New York, 1998.
- [25] N. M. Shapiro and M. Campillo, Emergence of broadband Rayleigh waves from correlations of the ambient seismic noise, *Geophys. Res. Lett.*, 31 (2004), L07614.
- [26] N. M. Shapiro, M. Campillo, L. Stehly and M. Ritzwoller, High resolution surface wave tomography from ambient seismic noise, *Science*, 307 (2005), 1615-1618.
- [27] R. Snieder, K. Wapenaar and U. Wegler, Unified Green's function retrieval by cross-correlation; connection with energy principles, *Phys. Rev. E*, 75 (2007), 036103-1-14.
- [28] D.-J. Van Manen and J. O. A. Robertsson, Modeling of wave propagation in inhomogeneous media, *Phys. Rev. Lett.*, 94 (2005), 164301.
- [29] K. Wapenaar, Synthesis of an inhomogeneous medium from its acoustic transmission response, *Geophysics*, 68 (2003), 1756-1759.
- [30] K. Wapenaar, Retrieving the elastodynamic Green's function of an arbitrary inhomogeneous medium by cross correlation, *Phys. Rev. Lett.*, 93 (2004), 254301-1,4.
- [31] K. Wapenaar, J. Fokkema and R. Snieder, Retrieving the Green's function in an open system by cross correlation: a comparison of approaches (L), *J. Acoust. Soc. Am.*, 118(5) (2005), 2783-2786.
- [32] R. L. Weaver, On diffuse waves in solid media, *J. Acoust. Soc. Am.*, 71 (1982), 1608-1609.